# Acoustic Oceanographic Buoy testing during the MREA'03 sea trial

C. Soares[1], S.M. Jesus[1], A. J. Silva[1], and E. Coelho[2]

[1] SiPLAB-FCT, Universidade do Algarve, PT-8005-139 Faro, Portugal.

[2] SACLANT Undersea Research Centre, I-19138 La Spezia, Italy

**Abstract**

This paper proposes an innovative concept that responds to the requirements of acoustic REA as the integration between a network of sophisticated Acoustic-Oceanographic Buoys (AOB) and online ocean properties inversion algorithms. A prototype of the system, including one sonobuoy and a preliminary version of the inversion code, was tested at sea during the MREA'03 sea trial. The AOB is a light acoustic receiving device that incorporates last generation technology for acquiring, storing and processing acoustic and non-acoustic signals received in various channels along a vertical line array. During the MREA'03 the AOB was deployed on a free drifting configuration. Source/receiver geometry was estimated from the buoy's GPS. Online processing was made possible by wireless transfer of the data and inversion was done in a range-dependent environment. Temperature profiles inverted from acoustic signals in two frequency bands on near real-time are shown to approximately agree with concurrent CTD measurements.

**Keywords:** sonobuoys, acoustic REA, ocean tomography

## I. INTRODUCTION

Ocean acoustic tomography (OAT) is an acoustic remote sensing technique for retrieving either bottom or water column ocean properties on real time. The OAT classical setup is made of a sound source emitting coded signals that propagate through the ocean and are received on a multiple sensor vertical line array. The estimation of the ocean properties of interest is posed as an inverse problem, where the propagation channel is parameterized according to an underlying physical model.

OAT can bring interesting advances to Rapid Environmental Assessment (REA) as the result of acoustic inversions can be assimilated into ocean circulation models tailored and calibrated to the scale of the area under observation. Traditional ocean tomography systems for their requirements of long and well populated receiving arrays and precise knowledge of the source/receiver geometries are not well adapted to operational Acoustic REA (AREA). To make AREA operational, the hardware involved in the reception of the acoustic signals must be light and handy. AREA must also be able to assimilate *a priori* environmental knowledge such as seafloor properties, bathymetry and telemetry data like GPS positions and acoustic source depth. Another component, intimately linked to the inversion process, is a collection of techniques, coming from signal and array processing, used to efficiently carry out parameter estimation. In order to respond to the above requirements, an innovative concept of AREA is being proposed under a NATO Undersea Research Centre (NURC) Joint Research Project, named AOB-JRP, formaly starting in 2004[1]. That concept includes the development of water column and geo-acoustic inversion methods being able to retrieve environmental true properties from signals received on a drifting network of Acoustic-Oceanographic Buoys (AOB). A prototype of an AOB and a preliminary version of the inversion code, was tested at sea during the Maritime Rapid Environment Assessment'2003 sea trial (MREA'03) and is described in this report together with the onboard inversion results obtained.

## II. THE ACOUSTIC OCEANOGRAPHIC BUOY

### A. AOB hardware

The AOB is a light acoustic receiving device that incorporates last generation technology for acquiring, storing and processing acoustic and non-acoustic signals received in various channels along a vertical line array. The physical characteristics of the AOB, in terms of size, weight and autonomy, will tend to those of

a standard sonobuoy, with however the capability of local data storage, processing and online transmission. Data transmission is ensured by seamless integration into a wireless LAN network, which allows for network tomography within ranges up to 10/20 km. There were only four acoustic channels in this first AOB prototype. The system bandwidth reaches 15 kHz which allows its usage in other applications, such as, active sonar and underwater communications. A simplified schematic is shown on figure 1.
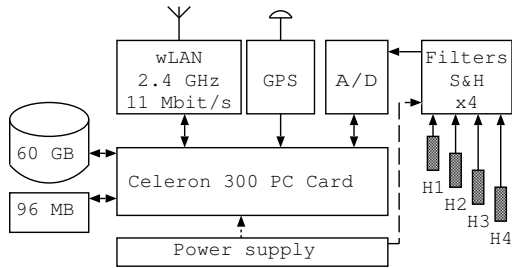


Fig. 1. *Block scheme representing Acoustic Oceanographic Buoy .*

The core of the AOB is a single board robust PC based on a Celeron 300 MHz with 256 MB RAM, a 96 MB chip disk with the operating system, another 60 GB hard-disk for data storage, output connectors for 10/100 Mb/s ethernet, USB, serial and parallel ports and video, mouse and keyboard connectors for monitoring and setup. A PCI/ISA (PISA) architecture was adopted so as to accommodate three other boards: the GPS board for 1 $\mu$s precision timing and localization of the buoy, a PCI interface for the 11 Mbit/s wireless LAN PCMCIA, and a high speed 16 bit ADC board for acoustic channels data acquisition. The 4 acoustic channels are led into their respective sample and hold filters, whose, on the other end are captured by the A/D card. The AOB has a cylindrical stainless steel body with top and bottom nylon covers through which the main internal components can be accessed via water tight connectors. In order to avoid electronic equipment damage by severe deck and crane banging during deployment/recover, the system was designed to be deployed switched off and automatically activates itself 2.5 minutes after deployment. The hydrophone array independently held the four hydrophones at nominal depths of 15, 60, 75 and 90 m. A 25 kg ballast was located at the array bottom end so as to maintain the array as much close to the vertical as possible.

## B. The AOB software

An important item to be tested during the MREA'03 sea trial was the AOB computer code to online control, monitor and invert the data collected with the AOB. In this preliminary test the software was separated in two parts: the sonobuoy control and monitoring and the online data inversion. The sonobuoy control and monitoring was performed by a specially developed Windows OS oriented program running on a laptop. This computer was fitted with a PCMCIA wireless card attached to an omnidirectional 12 dBi outdoor antenna via a 1 W amplifier. This computer code was performing two main tasks: one was to get the GPS location of the buoy and follow its drift in absolute coordinates from which the test area bathymetry was retrieved using archival data of the area. The second task was to monitor the data being acquired via a specialized program interacting with the buoy PC via Windows message passing protocol, over the wireless network. It was also possible to transfer acoustic data via ftp for on board online inversion. That data was shared on the network to a multiprocessor host devoted to data inversion. To carry out the data inversion in nearly real-time, a Dual AMD 2000+@1.667 GHz CPU rackmount computer running Linux was used.

The inversion software was based on code previously developed for Blind Ocean Acoustic Tomography (BOAT) [1], [2] with different settings for the parameter search bounds and genetic algorithms (GA) conversion parameters taking into account that source position was approximately known and that only very few (4) hydrophones were available. Setup of the inversion parameters was done via simulations prior to the sea trial.

## III. THE MREA'03 SEA TRIAL

### A. Experimental setup

The MREA'03 sea trial took place off the west coast of Italy in the north Elba Island area, during June 2003 and involved the R/V Alliance. The AOB was deployed on 21 June with very favorable weather conditions in an area of mild range-dependency. Fig. 2 shows the source-receiver geometry estimated from GPS recordings. The buoy was deployed at 11:01 local time and recovered at about 17:16. Source-receiver range varied between 500 up to 9 km. The bathymetric variability attained 20 m over some acoustic tracks, with 120 m waterdepth at buoy position and a maximum of 140 m waterdepth at source position. An acoustic source was deployed from R/V Alliance at a variable depth between 60 and 100 m depth, depending on ship speed. The objective of the acquired data was twofold: 1) to allow source localization using a single buoy with a few hydrophones in an unknown and range-dependent environment and 2) to perform tomographic inversions for the environmental parameters and therefore serve as input to the MREA experiment. Broadband LFM signals were transmitted using a lower frequency band (500-800 Hz) and a higher frequency band (900-1200 Hz) with a 2 s duration.
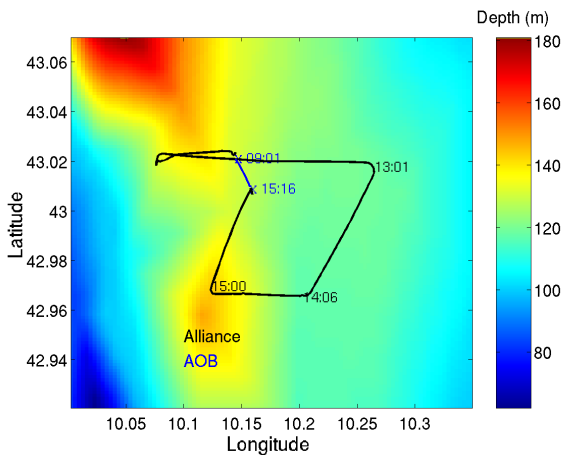
Fig. 2. *GPS estimated AOB and source ship navigation during the deployment of June 21.*
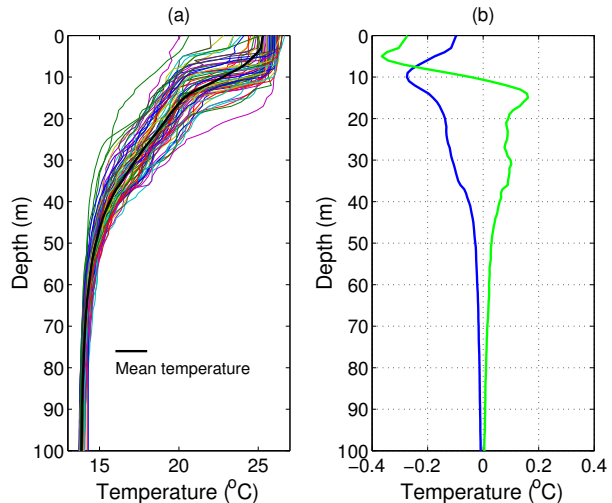


Fig. 3. *Recorded temperature profiles during days 16, 17 and 19 June. Mean profile is shown in thick black solid line (a); Two first Empirical Orthogonal Functions (b).*

Extensive ground truth measurements were performed before, during and after the deployment, including CTD measurements. For its relevance to the problem at hand, the temperature profiles collected during days 16, 17 and 19 of June are shown in Fig. 3(a), together with the two first Empirical Orthogonal Functions (EOF) (Fig. 3(b)), that account for 80% of the temperature variability during this period.

## IV. AREA USING AOB RECEIVED SIGNALS

### A. The environmental model

One of the tasks with largest impact in the final result, is the choice of an adequate environmental model to represent the propagation conditions of the experiment. This choice is generally the result of a compromise between a detailed, accurate and parameter full model and a light model ensuring a rapid convergence during the processing. The baseline computer model adopted for the MREA'03 was built based on the segmentation of archival bathymetric information along the source-receiver cross sections at different times. Geoacoustic properties were drawn from previous studies in the area [3] or historical databases. It consisted of an ocean layer overlying a sediment layer and a bottom half space with the bathymetry assumed to be range-dependent, as shown in Fig. 4. For the purposes of the inversion the forward model was divided into two parameter subsets: geometric parameters and water column temperature parameters. The baseline sediment and bottom properties were those estimated in [3] (Fig. 4). Water column variability was characterized thanks to the CTD data acquired during the previous days as represented in Fig. 3(b) by a set of two EOFs using these data. Forward modeling was computed using the normal mode propagation model C-SNAP [4].
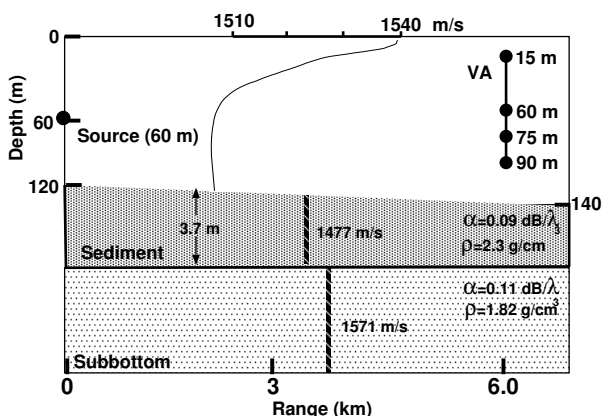
### B. The objective function



Fig. 4. *Baseline model for the MREA'03 experiment. All model parameters are range independent except water depth.*

The objective function used in this study is based on the cross-frequency Bartlett processor proposed in Soares *et al.* [5], and briefly described below. Let us assume the broadband model

$$
\begin{aligned}
\mathbf{Y}(\theta_0) &= [\mathbf{Y}^T(\theta_0, \omega_1), \mathbf{Y}^T(\theta_0, \omega_2), \cdots, \mathbf{Y}^T(\theta_0, \omega_K)]^T \\
&= \mathbf{H}(\theta_0)\mathbf{S} + \mathbf{U} \qquad (1)
\end{aligned}
$$

where $\mathbf{Y}(\theta_0)$ is the observed data vector at all hydrophones and at all discrete frequencies in the band, $\mathbf{H}(\theta_0)$ represents the acoustic channel transfer function assumed time invariant during $T$, with $T \leq 1/2N f_{\max}$ and $f_{\max}$ is the maximum frequency in the signal of interest, $\mathbf{S}$ is the source emitted signal spectrum and $\mathbf{U}$ is an additive noise term assumed to be zero mean and white. The

broadband cross-frequency matched-field processor is then given by

$$P(\theta) = \frac{\text{tr}\{\mathbf{P}_H \mathbf{C}_{YY} \mathbf{P}_H \mathbf{C}_{YY}\}}{\text{tr}\{\mathbf{P}_H \mathbf{C}_{YY}\}}, \qquad (2)$$

where $\mathbf{P}_H = \mathbf{H}(\theta)[\mathbf{H}^H(\theta)\mathbf{H}(\theta)]^{-1}\mathbf{H}^H(\theta)$ is a projection matrix, and $\hat{\mathbf{C}}_{YY}(\theta_0) = \frac{1}{N}\sum_{n=1}^{N}\mathbf{Y}_n(\theta_0)\mathbf{Y}_n^H(\theta_0)$ is the sample correlation matrix computed from $N$ snapshots. The $\mathbf{Y}(\theta_0, \omega_k), k = 1, ..., K$ are normalized before carrying out the averaging of the outer product, and $\hat{\mathbf{C}}_{YY}(\theta_0)$ has also norm 1. It was previously shown that this processor has identical performance than the coherent matched phase processor [6] and is well suited for low signal-to-noise ratio situations with high ambiguity and large frequency bandwidth.

## C. Acoustic tomography results

| Model parameter | Min | Max | Step |
|---|---|---|---|
| **Geometric** | | | |
| Source range (km) | $R_s$ - 0.3 | $R_s$ + 0.3 | 128 |
| Source depth (m) | $Z_s$ - 3 | $Z_s$ + 3 | 16 |
| Receiver depth (m) | 85 | 95 | 64 |
| Tilt (rad) | -0.045 | 0.045 | 64 |
| **Watercolumn** | | | |
| $\alpha_1$ ($^oC$) | -15 | 15 | 128 |
| $\alpha_2$ ($^oC$) | -15 | 15 | 128 |

TABLE I

*Inversion of acoustic data: GA forward model parameters, search bounds and quantization steps. Search intervals for source range and depth are centered on GPS values.*

Acoustic inversion was attempted on the data collected on June 21$^{st}$ on both frequency bands transmitted. The time elapsed between pings was 10 minutes for the lower frequency band, and 20 minutes for the higher frequency band. In the processing, the sampled signals were decimated to 2.008 kHz and 4.016 kHz, for the low and high frequency bands, respectively, while 22 equispaced frequency bins were taken in each band. To compute the sample correlation matrices 10 snapshots were considered. It took about 4 days to carry out 12 inversions in the lower frequency band and 6 inversions in the higher frequency band. This was particularly long due to the large frequency bands being considered and the range dependency of the environment.

Table I shows the search parameters, their respective intervals and number of quantization steps when optimizing with the GA. The search interval for source range



Fig. 5. *Inversion results for ocean temperature in two frequency bands: 500-800 Hz (blue); 900-1200 Hz (red).*

and depth is always centered in the true GPS values and the bounds are relatively tight so as to allow only slight adjustments of possible position measurement errors. Another reason for using tight bounds is the extremely high ambiguity between source range and EOF coefficients seen during the previous simulation study. The number of generations was set to 50 with 190 individuals and 3 independent populations. The mutation and cross-over probabilities were respectively set to 0.0056 and 0.9. The populations were initiated using the previously estimated parameter vector: 30% of the individuals are initialized in an interval centered on the previous estimate with a search amplitude which is 10% of the total interval. The estimated temperature profiles are shown in Fig. 5. It can be seen that the temperature profiles obtained in the lower frequency band show high variability resulting in unlikely estimates through time (blue curves). The temperature estimates at the surface are between 21 and 30 $^oC$, which is very unlikely even if both time and space dependence is taken into account. On the other hand the variability of the estimates obtained on the higher frequency band (red curves) is clearly lower, where the temperatures at the surface vary within more reasonable bounds of 23
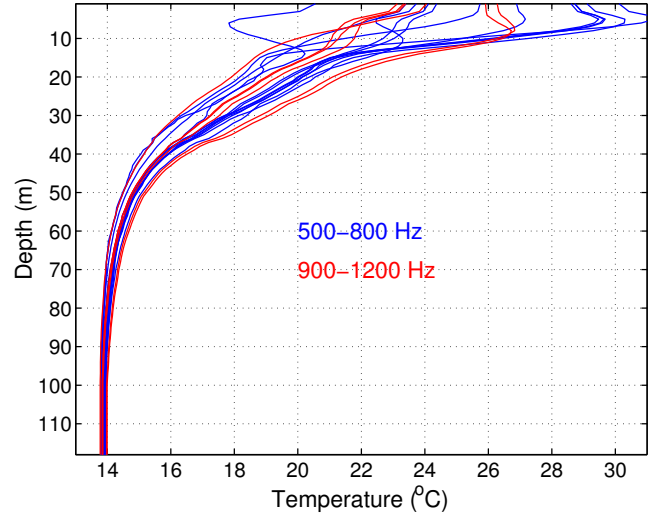
to 26.5$^o$C$^2$ with, however, the estimates of the $\alpha_i$ suffering unlikely variations. In order to try to understand the challenge posed by the problem of estimating two EOF coefficients on an uncertain environment and how does it varies with frequency, a short simulation was performed. In that simulation the baseline model of Fig. 4 was considered with the acoustic source located at 6 km range and 60 m depth and a water depth of 120 m. The synthetic data is noiseless and all cross-frequency terms have the same weight. Fig. 6 shows the EOF coefficients $\alpha_1$-$\alpha_2$ error ambiguity surfaces for the lower (a) and higher frequency bands (b), respectively. The generally assumed behavior that ambiguity decreases with frequency is not verified in this case. In fact, the result obtained in the higher frequency band (b) has a more pronounced diagonal than that in the lower frequency band (a). But if, for example, a source range mismatch of 300 m is encountered, the relative performance in the two bands may be altered as shown in Fig. 6 (c) and (d) for the lower and upper frequency bands, respectively. It is verified that in both cases the surface maxima are shifted towards higher values of $\alpha_1$. These pictures also reveal that the relative surface ambiguity has changed: now the lower frequency band is more degraded than that obtained in the higher frequency band. From this test it appears that the high frequency band is more robust to source range mismatches. Another important factor that distinguishes the two frequency bands is the noise level. In terms of sidelobes, white noise would have the harmless effect of adding a constant to the surface, while correlated noise would desiquilibrate the main peak to sidelobe ratio, deviating the estimate to an unpredictable location. Fig. 7 shows a noise spectrum estimate (a) and the cross-frequency spectrum (b), using raw data. The noise was observed during 80 s at the shallowest hydrophone. Then an averaged periodogram was computed by dividing the observed noise signal into windows of 0.5 s, giving 160 snapshots. In plot (a) it can be seen that the estimated noise level falls off more than 7 dB in the band from 500 to 1200 Hz, showing a slight hyperbolic arch. This estimate seems to be roughly in agreement with the noise spectrum Venz curves from Urick [7], but with a slightely higher attenuation. Plot (b) shows the corresponding cross-spectrum which gives a better idea of noise cross-correlation extent being used in the cross-frequency processor. In order to avoid the noise power dependence and to have better estimation of the noise frequency cross-correlation, the element $ij$ of the matrix $\mathbf{C}_{NN}$ can be divided by $\sqrt{\mathbf{C}_{NN}(\omega_i)\mathbf{C}_{NN}(\omega_j)}$, which results in a matrix with all ones in the diagonal. Plot (b) clearly shows that the degree of decorrelation increases with frequency which could eventually determine the performance that can be attained on one or on the the other frequency band.

### D. Source localization

In the above performance of OAT, it was assumed that the source location was known with an high degree of accuracy, and therefore tight search bounds have been chosen. Thus, the possibility of mislocation the source is artificially restricted, and it becomes uncertain whether the model estimates is in agreement with the reality. An environmental model test can be recast in the form of a range-depth source localization problem, since range and depth are leading parameters during the GA search process. Conversely, if the environmental model is not correctly estimated, then the source cannot be correctly located during a localization search. Fig. 8 shows the source location estimates using the previously estimated model parameters, tilt, hydrophone depth and EOF coefficients. The asterisks indicate the estimates obtained with the tight boundaries during environmental inversion, the circles are the range-depth estimates, with blue color corresponding to the lower frequency band, red color corresponding to the higher frequency band. For the lower frequency band severe errors were obtained for 5 out of 12 estimates. For the higher frequency band the quality of the range-depth estimation is significantly better with only one severe estimation error. In principle this test should allow wrong

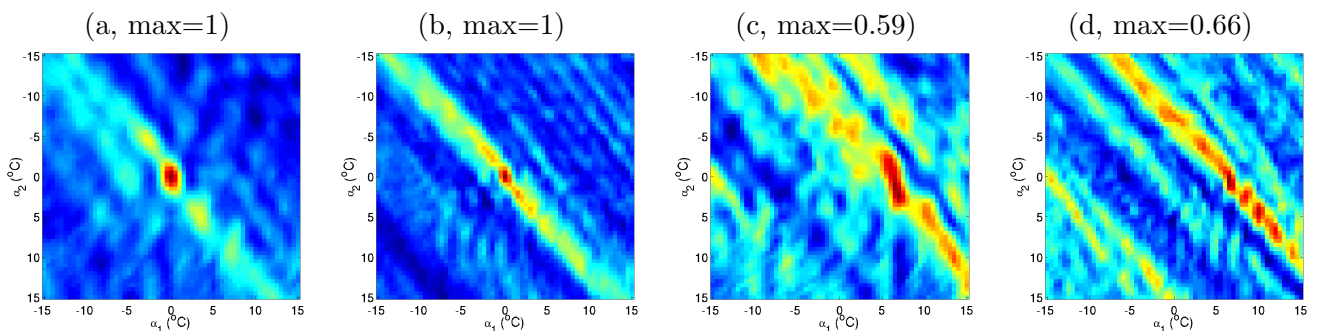$^2$surface temperature of the CTD data shown on Fig. 3 varies between 25 and 27$^o$C.



Fig. 6. *Simulated data with the baseline model $\alpha_1$-$\alpha_2$ error ambiguity surfaces in the frequency band 500-800 Hz: without mismatch (a) and with 300 m source range mismatch (c) and in the frequency band 900-1200 Hz: without mismatch (b) and with 300 m source range mismatch (d).*
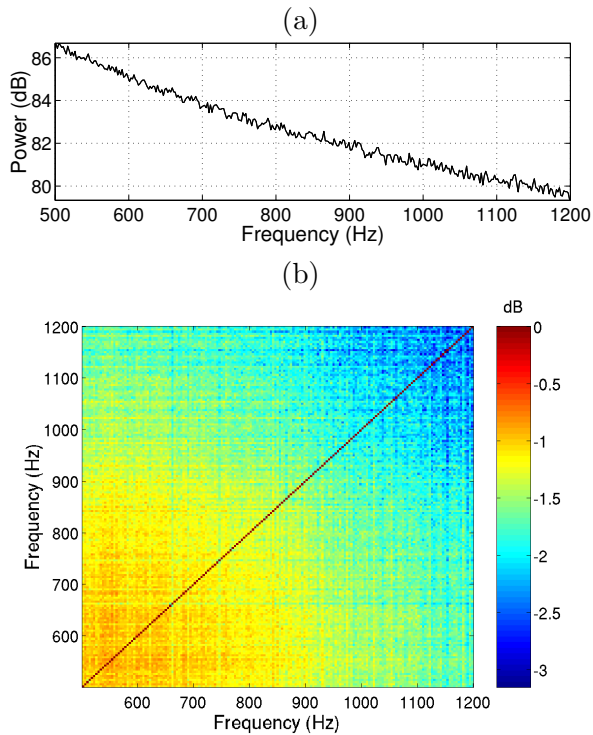
Fig. 7. *Noise spectrum estimated with acoustic data taken at the shallowest hydrophone: periodogram (a) and cross-frequency power spectrum (b).*
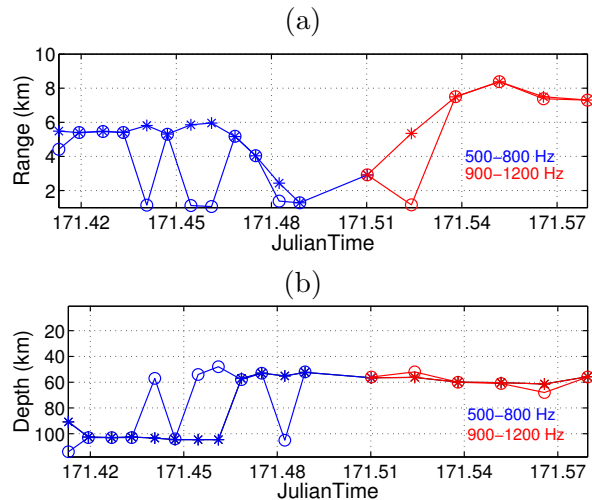


Fig. 8. *Source localization using the estimated environmental parameters: source range (a) source depth (b). (∗) GA estimates obtained with tight boundaries; (o) source localization estimates.*

environmental models estimates to be discarded. However, in this case it appears that model mismatches can not always be associated with source-localization errors. In the present case the main-to-sidelobe ratio is so weak that a small mismatch or noise can potentially change the position of the maximum. On the other hand, the example shown in Fig. 6 suggests that at a low SNR several pairs $(\alpha_1, \alpha_2)$ can have a similar MF response.

## V. Conclusions and future developments

The MREA'03 sea trial constituted an opportunity for testing an AOB prototype and an initial set of inversion algorithms. The concept of a light and fully operational acoustic buoy has been proven successful, where monitoring was possible up to a range of approximately 9 km. From the hardware point of view, this test indicated that the concept is feasible, i.e., a small and light system can be developed to acquire, process, store and transmit acoustic and oceanographic data for REA purposes. The embedded PC technology and its wireless LAN philosophy is to be pursued. The size and weight of the buoy can be reduced and the number of acoustic and oceanographic channels can and should be increased. On the online acoustic inversion side it was shown that it is indeed possible to invert acoustic data from a free drifting operational buoy. However, it was also shown that the number of existing acoustic channels is clearly not sufficient for a reliable water column inversion. It was also shown that, at least with four acoustic channels, a frequency band centered in 1.050 kHz provided more robust and reliable results than a lower band around 650 Hz.

## References

[1] S. M. Jesus, C. Soares, J. Onofre, and P. Picco. Blind ocean acoustic tomography: experimental results on the intifante'00 data set. In *Proc. of the European Conference of Underwater Acoustics*, Gdansk, Poland, June 2002.

[2] S. M. Jesus, C. Soares, J. Onofre, E. Coelho, and P. Picco. Experimental testing of the blind ocean acoustic tomography concept. In *Impact of Littoral Environmental Variability on Acoustic Predictions and Sonar Performance*, Lerici, Italy, September 2002.

[3] C. Soares, A. Waldhorst, and S. M. Jesus. Matched-field processing: environmental focusing and source tracking with application to the North Elba data set. In *Oceans'99 MTS/IEEE Proceedings*, volume 3, pages 1598–1602, Seattle, 1999.

[4] C. M. Ferla, M. B. Porter, and F. B. Jensen. C-SNAP: Coupled SACLANTCEN normal mode propagation loss model. Memorandum SM-274, SACLANTCEN Undersea Research Center, La Spezia, Italy, 1993.

[5] C. Soares and S. M. Jesus. Broadband matched field processing: Coherent and incoherent approaches. *J. Acoust. Soc. Am.*, 113(5):2587–2598, May 2003.

[6] G. J. Orris, M. Nicholas, and J. S. Perkins. The matched-phase coherent multi-frequency matched field processor. *J. Acoust. Soc. Am.*, 107:2563–2575, 2000.

[7] R. J. Urick. *Principles of Underwater Sound.* McGraw-Hill, New York, 1983.